BIOPHYSIQUE À L'ÉCHELLE DE LA MOLÉCULE UNIQUE
SINGLE MOLECULE BIOPHYSICS

Single-molecule spectroscopy and microscopy

Xavier Michalet *, **Shimon Weiss**

Department of Chemistry and Biochemistry, UCLA, 607, Charles E. Young Drive East, Los Angeles, CA 90095, USA

Abstract   Advances in detector sensitivity and improvements in instrument design have recently provided scientists with tools to probe single molecules with light, and monitor their photophysical properties with exquisite sensitivity and spatial as well as temporal resolution. Spectroscopic and temporal information is used to explore molecular structure, conformational dynamics, local environment and intermolecular interactions of individual species. High-resolution single-molecule microscopy allows these methods to be used for in vitro or in vivo molecular colocalization with nanometer precision. The collected data have generated a wealth of new information in domains ranging from chemistry and biology to solid state physics. ***To cite this article: X. Michalet, S. Weiss, C. R. Physique 3 (2002) 619–644.***
© 2002 Académie des sciences/Éditions scientifiques et médicales Elsevier SAS

single molecule / spectroscopy / fluorescence / fluorophore / confocal microscopy / near-field scanning optical microscopy / lifetime / polarization / fluorescence resonance energy transfer / polymer dynamics / enzyme dynamics

Spectroscopie et microscopie d'une molécule unique

Résumé   Des progrès récents sur le plan de la sensibilité des détecteurs et de la conception des expériences permettent d'étudier les propriétés photophysiques de molécules uniques avec une sensibilité et des résolutions spatiale et temporelle optimales. Les données spectroscopiques et temporelles permettent d'accéder à la structure moléculaire, aux changements conformationnels, aux interactions intermoléculaires et à la nature de l'environnement d'une molécule unique. L'extension au domaine de la microscopie permet d'étudier la colocalisation de molécules uniques in vitro et in vivo avec une résolution de l'ordre du nanomètre. Ces avancées bénéficient autant à la chimie qu'à la biologie ou à la physique. ***Pour citer cet article : X. Michalet, S. Weiss, C. R. Physique 3 (2002) 619–644.***
© 2002 Académie des sciences/Éditions scientifiques et médicales Elsevier SAS

molécule unique / spectroscopie / fluorescence / fluorophore / microscopie confocal / microscopie optique à balayage en champ proche / durée de vie / polarisation

* Correspondence and reprints.
  E-mail addresses: michalet@chem.ucla.edu (X. Michalet); sweiss@chem.ucla.edu (S. Weiss).

DOSSIER

Abbreviations

APD: Avalanche Photodiode

CCD: Charge-Coupled Device

CW: Continuous Wave

DNA: Deoxyribonucleic Acid

FRET: Fluorescence Resonance Energy Transfer

GFP: Green Fluorescent Protein

NA: Numerical Aperture

NC: Nanocrystal

NSOM: Near-Field Scanning Optical Microscopy

PMMA: Polymethylmethacrylate

PMT: Photomultiplier Tube

QE: Quantum Efficiency

SERS: Surface-Enhanced Raman Scattering

SMS: Single-molecule Spectroscopy

SNR: Signal-to-Noise Ratio

SBR: Signal-to-Background Ratio

TIR: Total Internal Reflection

ZPL: Zero-Phonon Line

1. Introduction

With the completion of sequencing projects of several organisms, the continuous accumulation of protein structures and the elucidation of biochemical pathways, scientists are progressively achieving what could be described as an index of the book of life. However, life is a dynamic process unfolding in three dimensions, and there still remains the daunting task of fully describing the spatio-temporal location and conformation of all these indexed components, as well as their complex interactions. Techniques using gene- or protein-chips, X-ray diffraction, NMR, yeast two-hybrid, phage display, etc., allow part of this information to be uncovered, but they lack the sensitivity needed to unravel the details and dynamics of individual molecular events. The reason is that these measurements performed on ensembles of molecules are statistical and often static by design: they only yield average information, concerning final stages of reaction paths or conformational changes. These averaging processes are several-fold: averages over molecular heterogeneity (e.g. chemical composition or spatial conformation) and averages over different or changing local environments. Dynamic processes studied by ensemble measurements cannot separate molecules exhibiting fast or slow reaction times, although such differences are expected from the stochastic nature of any chemical process. Moreover, since synchronization of an ensemble of molecules is hard

to achieve and impossible to maintain, individual molecular dynamics and kinetics are rarely accessible. To disentangle the contributions of these various factors, it is crucial to be able to probe the behavior of individual molecules. This can be done by isolating molecules (e.g. by dilution) or by using a probing method that is effectively site or molecule specific.

Optical spectroscopy methods are especially adapted to this purpose, for their non-invasiveness and sensitivity to molecular conformation and environment, via changes in the electronic structure. At cryogenic temperatures, spectroscopic studies of single molecules and their evolution under the influence of different external parameters allow precise tests of molecular quantum electrodynamics and microscopic theories of coupling with their environment [1,2]. At higher temperature, they give access to the temporal evolution of different nanodomains of a bulk material (crystal, glass) in which single molecules are embedded as reporters of their environment [3,4]. In biological and biochemical processes, whose building blocks are often individual molecules (ribonucleic acid – RNA – molecules, enzymes, motor proteins, etc.), the ability to fully understand their dynamic behavior at the single-molecule level is of outmost importance [5–7]. Developments of reliable and versatile fluorescent labeling techniques have made most of these molecular events amenable to microscopic observation at the single-molecule level [8]. Finally, nanometer resolution imaging and single photon-emitter detection is a prerequisite of the full development of the promises of nanotechnology and quantum computing [9]. Single-molecule experiments and methods have thus pervaded an ever increasing number of research fields.

This article reviews single-molecule spectroscopy and microscopy (SMS) techniques and applications, focusing mainly on the fluorescence emanating from a single emitter (fluorophore). After a historical overview presented in Section 2, the principles underlying single-molecule fluorescence spectroscopy approaches are introduced in Section 3. Section 4 covers important photophysical properties of molecules and presents microscopic and spectroscopic approaches available to the experimentalist. Section 5 describes some applications of these techniques, focusing on physical properties of materials and biological applications of single-molecule spectroscopy. The last part briefly outlines the future prospects of single-molecule approaches. A number of recent reviews [2,5,10,11,13,14] or books [10,15,16] can be consulted for complementary points of view.

2. Historical overview

The first (though unsuccessful) attempt to probe individual fluorescent molecules is probably due to Jean Perrin almost a century ago [17]. Although E.A. Synge proposed an experimental scheme allowing in principle the performance of nanometer resolution microscopy in 1928, thus predating near-field optical microscopy by over 50 years [18–20], single-molecule measurements were first successfully performed with non-optical methods. For instance, the patch clamp technique developed by Neher and Sackmann allowed recording of ion translocation through a single ionic channel embedded in a cell membrane [21]. Later on, scanning tunneling [22] and atomic force microscopy [23] opened the way to molecular scale investigations on surfaces [24,25], complementing electron microscopy. Only recently have optical methods reached the sensitivity required to detect [26,27], image [28], manipulate [29] and follow the spectroscopic evolution of single fluorophores on surfaces [30], in solids [31], liquids [32] and fluid membranes [33] as well as inside live cells [34,35].

Single-molecule spectroscopy was initially demonstrated in a system of pentacene molecules embedded in a *p*-terphenyl host crystal at liquid helium temperature [1,26]. Absorption spectroscopy in this system takes advantage of the narrow zero-phonon absorption line (ZPL) of the rigid pentacene molecule, corresponding to the transition from the electronic ground state to the first excited state. The position in laser-frequency space of each molecule's ZPL indeed depends on the local fields, allowing for a precise molecular selectivity. However this approach is limited to few molecule–host pairs and requires cryogenic temperatures due to broadening of the ZPL above 10 K. A more convenient variant of this approach was developed soon thereafter, using fluorescence emission spectroscopy [27,31]. The ability to separate the

Stokes-shifted fluorescence emission from the excitation resulted in a larger signal-to-noise ratio. These molecule-host pair systems have been recently studied at room temperature, providing different types of information [36,37].

The successful detection of a single antibody molecule labeled with ~ 100 fluorophores by total internal reflection (TIR) microscopy was first demonstrated by Hirschfeld in 1976 [38]. Single fluorophore detection at room temperature was first achieved using standard flow-cytometry methods [32,39]. Single molecules randomly passing through the excitation volume gave rise to sudden bursts of photons emitted during their brief transit. Initially developed for rapid DNA sequencing, this simple approach is now widely used for more sophisticated studies in its confocal version [40], and benefits from developments in fluorescence correlation spectroscopy (FCS) [41,42].

The first image of a single molecule at room temperature was obtained using near-field scanning optical microscopy (NSOM) [28], rapidly followed by similar achievements using far-field confocal microscopy [43] trading spatial resolution for enhanced ease-of-use. These approaches based on sample scanning have advantages and disadvantages that will be discussed in the following. TIR and wide-field epifluorescence imaging are now efficiently used to image and study the two-dimensional and three-dimensional diffusion trajectories of single fluorescent molecules [33–35].

3. Requirements for single-molecule sensitivity

3.1. Detection: signal, background and noise

Observing single molecules may be as challenging as finding a needle in a haystack if background, signal and noise are not carefully optimized. Fig. 1 illustrates simple principles involved in single-molecule optical excitation and detection. Photon absorption leading to fluorescence emission is chiefly characterized by a cross section σ and fluorescence emission by a quantum yield Q (number of emitted photons per absorbed photon). The optical setup transmits an excitation power P at a frequency v, resulting in a signal rate $s = EQ\sigma P/Ah\nu$ expressed in counts per second (cps or Hz). This rate is proportional to P/A where A is the cross section of the excitation beam in the plane of the molecule. E is the collection efficiency of the setup. The environment adds a background rate b per unit-volume and unit-excitation power (due to remnant Raman or Rayleigh scattering, fluorescence of the substrate or of the detection optics, etc.), and the detector, a dark count rate d. A first important quantity is the signal-to-background ratio (SBR):

$$SBR = \frac{EQ\sigma}{bVAh\nu}. \tag{1}$$

If the noise from the readout electronics can be neglected (it is independent from the integration time), a measurement of duration τ will yield the following signal-to-noise ratio (SNR):

$$SNR = \frac{s\tau}{\sqrt{(s + bVP + d)\tau}}, \tag{2}$$

where V is the excited volume. The denominator is the root mean square of all contributions to the shot-noise (a shot-noise limited signal follows a Poisson distribution, whose variance equals its mean value). The SNR obviously increases at larger integration time τ. For negligible dark count rate,

$$SNR = \sqrt{s\tau}\left(1 + SBR^{-1}\right)^{-1/2}. \tag{3}$$

A large SBR results in an optimal SNR which depends only on the count rate s and integration time τ. A poor SBR reduces the SNR compared to this optimal value. Both ratios can be increased by improving the collection efficiency E, and the SBR can be further improved by decreasing the excitation volume V. A larger excitation power (as long as saturation is not reached, see Section 4.2) or a longer integration
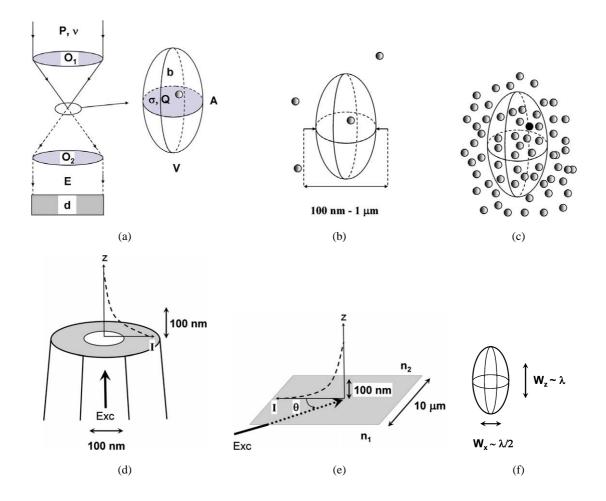
Figure 1. Signal, background and noise issues in single-molecule detection. (a) In a single-molecule spectroscopic experiment, excitation light (power P, frequency ν) is focused on the sample through an optical element O_1 (objective lens, fiber tip), exciting a diffraction-limited volume of cross section A, represented by an ellipsoid in the expanded view. The absorption process is characterized by an absorption cross section σ and the emission by a quantum yield Q. The background contribution per watt of incident power is b, whereas the detector will have a dark count rate d. The signal is collected by an optical element O_2 (possibly confounded with O_1), and further guided to the detector, with an overall efficiency E. (b) The signal of a single molecule can be separated from that of other molecules if the probability to find two or more molecules in the probed volume is negligible. This can be obtained either by a low concentration, or by reducing the excitation volume. (c) If each molecule in the excited volume can be characterized by a different spectral property (which can depend or not on its exact environment), it is possible to use very selective excitation or detection techniques to probe just one molecule in the sampled volume (the black sphere in the ellipsoid). (d) Excitation volume for a NSOM setup. The near field decays exponentially over a few tens of nanometers away from the tip aperture (diameter ~ 100 nm). It strongly depends on the tip shape and surface distance, as well as input polarization among other parameters [28]. (e) Excitation volume for a TIR setup. The evanescent field decays exponentially away from the interface with a decay length $d = \lambda/4\pi (n_1^2 \sin^2 \theta - n_2^2)^{1/2} \sim \lambda/5$, where n_1 is the glass refraction index, n_2 the liquid (or air) refraction index, and θ the angle of incidence of the totally reflected beam. The lateral extent of the excitation depends on the beam expansion [128]. (f) Excitation volume in a confocal setup. The full widths at half maximum for non polarized light are (scalar approximation): $W_x = 0.51\lambda/NA \sim \lambda/2$ and $W_z = 0.44\lambda/n \sin^2(\alpha/2) \sim \lambda$, where $NA = n \sin \alpha$ is the numerical aperture [52].

time will improve the *SNR* without affecting the *SBR*. The value of the residual background rate b can be reduced by a careful choice of buffer, embedding matrix or immersion medium, and rejection filter or use of a confocal design.

Typical values for the above parameters in the case of a confocal microscopy study of freely diffusing fluorescein isothiocyanate (FITC) in water, using silicon avalanche photodiode detectors (APD) are: $E = 10^{-2}$, $Q = 0.85$, $\sigma = 2.8 \cdot 10^{-16}$ cm^2, $A = 1$ μm^2, $\lambda = 525$ nm, $bV = 100$ Hz/μW, $d = 100$ Hz. With an excitation power of 100 μW and a 1 ms integration time, a count rate of 73 counts/ms can be obtained, of which 7 come from the background sources, leading to a *SNR* ~ 7 and *SBR* ~ 6. Although these are good figures, they have to be balanced by the fact that single molecules have a finite life span. Single molecules in an oxygen-rich environment typically emit on the order of 10^6 photons before irreversible degradation (photobleaching). With the above parameters, this amounts to a total emission of ~ 160 ms. This is enough to observe freely diffusing molecules during their transit time of a few hundred μs. For an immobilized molecule however, it sets a stringent limit on the total duration of a single-molecule observation, and all efforts are put on reducing the excitation volume and intensity, as well as background sources.

3.2. Criteria of singleness

In addition to *SBR* and *SNR* issues, care has to be taken to ensure that the collected signal originates from a single molecule. This is not just a purist's concern. As well designed as an experiment may be, there is always the possibility that two or more fluorescent molecules occupy the diffraction-limited excitation volume (typically, several hundred nanometers across, ~ 1 fl in volume). If intensity fluctuations (or variations of any other spectroscopic characteristics) are observed, they can be due to single-molecule dynamics, environment changes, but they could as well reflect the random mixture of emissions from nearby molecules. It is thus critical to eliminate this unneeded source of uncertainty. Two different strategies can be envisioned to limit this risk:

 (i) work at low concentration, such that at most one molecule is present in the excitation volume (Fig. 1(b)), or equivalently, minimize the excitation volume;
(ii) use a selective excitation or emission detection protocol, such that only one molecule is excited or detected within the sampled volume (Fig. 1(c)).

The first and most common strategy is for instance illustrated in the experiment presented in Fig. 2, in which a dilute solution of fluorescent molecules yields separate bursts corresponding most of the time to transits of individual molecules through the diffraction-limited focal spot of a microscope objective [44]. The second strategy requires fluorophores having either separable excitation or emission properties, and was adopted in the first pentacene/p-terphenyl ZPL studies evocated previously [26,27]. In these experiments, each pentacene molecule had a different, narrow peak absorption frequency depending on its microscopic neighborhood, to which the laser could be fine-tuned. Despite the large area excited by the laser beam, no other molecules were excited because they were all out of resonance, resulting in a clear single-molecule signal. The alternate scheme, in which nearby fluorophores are distinguished by their emission properties (e.g. fluorescence lifetime [45] or spectra [46,47]) will be illustrated with fluorescent semiconductor nanocrystals later on.

Once experimental conditions favoring single-molecule detection are satisfied, a number of criteria have to be met to ascertain that the observed signal actually comes from a single emitter [11,28]. These criteria, summarized in the following list, are direct consequences of common photophysical properties of fluorophores, which will be described in the next section:

  (i) The observed density of emitters is compatible with the known concentration of individual molecules and scales with the original bulk concentration.
 (ii) The observed fluorescence intensity level is consistent with that of a single emitting molecule.
(iii) Each immobilized emitter has a well-defined absorption or emission dipole (for organic dyes usually linear, but planar for other emitters such a fluorescent semiconductor nanocrystal [48]).
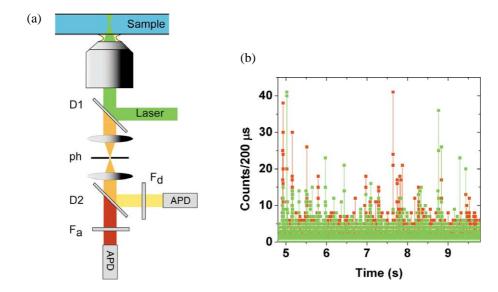
Figure 2. Single-molecule fluorescence burst detection. (a) Schematic of a confocal setup used for single-molecule fluorescence detection. A collimated laser beam is focused through a high *NA* objective in a liquid ccontaining chamber. Molecules diffusing through the diffraction-limited excitation volume (~ 1 fl) emit photons during their passage, which are collected by the same objective. A dichroic mirror (D1) separates excitation and emission wavelengths. The emitted light is focused on a pinhole (ph) in order to reject out-of-focus background light, and finally recollimated onto two different APDs after spectral separation by a dichroic mirror (D2). Filters specific for each channel (F_a: acceptor channel, F_d: donor channel) may be used to improve spectral separation. (b) 5 s time trace of recorded bursts for a 30 pM solution of doubly labeled DNA in 20 mM sodium phosphate buffer. The DNA constructs are used for distance measurement (detailed in Fig. 7) and have a TMR fluorophore attached to one end of the DNA molecule and a Cy5 fluorophore attached to the nth base from the end. The time traces correspond to $n = 12$. Green: TMR fluorescence (donor); red: Cy5 fluorescence (acceptor). The laser excitation (0.6 mW, 514 nm) is focused 10 μm within the solution through an oil immersion objective (numerical aperture: 1.4). For each detected photon, the APD generates a pulse, which is recorded by a computer-embedded acquisition board. Counting these events into 200 μs bins, the resulting time trace exhibits distinct bursts distributed randomly in time, with duration and amplitude corresponding to a Brownian diffusion of individual molecules through the excitation volume.
(b) *Adapted with permission from Ref. [44]. Copyright 1999, the National Academy of Sciences USA.*

(iv) Fluorescence emission exhibits only two levels (on/off behavior due to blinking or photobleaching) over time scales where no changes in the environment are expected [49].
(v) If there are two or more emission levels, photophysical property changes are correlated with blinking [50].
(vi) The emitted light exhibits antibunching, which is characteristic of a single quantum emitter [51].

The main source of ambiguity comes from blinking. A fluctuating, non-blinking intensity recording might come for instance from a single molecule that undergoes rotation, or whose environment changes over time. It might also come from the superposition of the blinking or fluctuating behavior of a few molecules. This latter case is easily detected on an antibunching curve: for several molecules, coincident emission of photons by the different molecules are likely and will result in an autocorrelation function that does not cancel out for zero time-delay. However, for a small number of blinking molecules (say, two), the total number of coincident emissions might be too low to reject the single-molecule hypothesis with the antibunching curve only. In this case, monitoring a photophysical property (spectrum, lifetime) simultaneously with the intensity fluctuations may resolve the issue. Indeed, for a set of two molecules having different photophysical properties (for instance, a different spectrum), observing repeated spectral

625

fluctuations consecutive to blinking events would require a perfect synchronization of the on/off switching of both molecules, an unlikely situation.
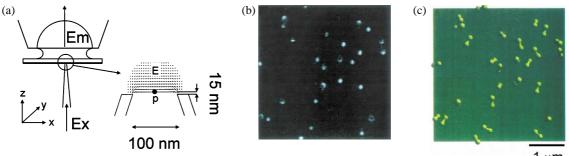
3.3. Embodiments

3.3.1. *Acquisition geometries*

The above constraints and criteria for single-molecule sensitivity and/or localization accuracy are fulfilled differently in the various types of acquisition geometries most commonly encountered. A first distinction can be made between point detection and wide-field detection schemes, and each category can be divided according to the chosen type of excitation and detection.

Point-detection schemes encompass confocal and near-field scanning optical microscopies. By construction, the excitation volume has a dimension of the order of the excitation wavelength for confocal microscopy (Fig. 2) [52], and of the tapered fiber core (~ 100 nm) for NSOM (Fig. 3) [20]. These geometries allow the acquisition of fluorescence time traces of immobilized molecules with high temporal resolution, as well as fluorescence lifetime information [43], but they are rather slow for imaging single molecules. They require a total time per frame proportional to the number of pixels in the image, with a typical time per pixel of the order of a few ms (required for good *SNR*). Confocal microscopy is also extensively used for the study of freely diffusing molecules in solution or embedded in fluid membrane (lipid bilayer of cell membranes) by FCS [41,42], as illustrated in Fig. 2.

Wide-field detection schemes use either epifluorescence illumination with lamps [53], defocused laser excitation [33], or TIR excitation [54,55]. Using wide-field imaging is necessary for particle tracking studies, but can also be preferred over single-point detection for simultaneous observation of separated individual molecules. This reduces the amount of time needed to accumulate a statistically significant number of observations. It is especially relevant for experiments in which irreversible processes are triggered by modification of an external parameter. Although they allow faster image acquisition than

Figure 3. Near-field scanning optical imaging of single molecules at room temperature. (a) Schematic of a near-field scanning optical microscope setup used for single-molecule imaging. An aluminum-coated tapered optical fiber (raster-scanned at nanometer distance from the sample) with a sub-wavelength aperture (5–10 nm) serves as a wave-guide for laser excitation. Shear-force feedback keeps the tip at a constant distance from the sample, resulting in a signal used for nanometer-resolution topographic reconstruction of the scanned area. The excitation volume and the corresponding local evanescent electric field are detailed in the expanded view. Fluorescence light emitted by individual molecules is collected by an oil immersion, high NA objective and recorded by an APD. (b) 4×4 μm^2 area of a polymethylmethacrylate (PMMA) coated coverslip on which a diluted methanol solution of a lipophilic carbocyanine dye, diIC$_{12}$, was deposited. Scanning was performed with randomly-polarized light. (c) Orientation of the corresponding individual emitting dipole determined by modeling the field distribution (expanded view in (a)), simulation of the absorption intensity with polarized excitation and comparison with data obtained at two different excitation polarizations.
(a) *Adapted with permission and* (b, c) *reprinted with permission from Ref.* [28]. *Copyright 1993, the American Association for the Advancement of Science.*

point detection setups because all pixel values are recorded simultaneously, readout noise effectively limits transfer rates to a few images per second. Higher frame-rates can be achieved when smaller regions of interest are studied [33,53].

3.3.2. *Detectors*

Similar considerations hold on the detector side, where a trade-off has to be made between time-resolution and quantum efficiency (QE). For instance, until recently, photomultiplier tubes (PMT) had a QE of 10–20% in the visible spectrum but very good time resolution ($\sim$ 20 ps) [56], whereas silicon APD have typical QE of 70% in the visible, but only $\sim$ 400 ps resolution. Both kinds of detectors, used in the photon-counting, mode have a maximum count-rate of a few MHz [57–59]. New progress in photocathode technology (using GaAsP photocathodes) should increase the QE of PMT to values closer to that of APDs, making them attractive detectors for beam scanning confocal microscopes because of their larger sensitive area.

For observation techniques based on wide-field detectors, back-thinned charge-coupled devices (CCD) have QE in the $\sim$ 90% range, but a usable readout rate limited to a few frames per second by readout noise (which should thus be included in Eq. (2)). Intensified CCDs (ICCDs) overcome the readout noise limitation by signal amplification, for instance with MCP, allowing higher frame rates, but at the price of a much lower QE (10–20%). The recently demonstrated Electron Multiplying CCD (EMCCD) technology should permit progress in frame-rate as high as 10 MHz [60]. Finally, although based on MCP technology (low QE), time-resolved 2D detectors provide subnanosecond temporal resolution, allowing lifetime as well as spectral information to be recorded simultaneously [61,62].

4. Types of spectroscopy and microscopy

4.1. Fluorophores

A variety of fluorophores have been investigated with single-molecule spectroscopy techniques. Fluorescent organic molecules [28], green fluorescent proteins (GFP) [63] and other fluorescent proteins [64,65], conjugated polymers (J-aggregates) [66], light-harvesting complexes comprising several fluorophores acting effectively as a one quantum emitter [67,68], dendrimers [69] or semiconductor nanocrystals (NCs) [70] are but a few examples of systems which have been extensively studied at cryogenic as well as at room temperature. Each of these systems exhibit fluorescence based on specific processes, which, for lack of space, cannot be described here [59]. Although initial experiments studied fluorophores for their own sake, SMS has now reached the stage where fluorophores can be confidently used as reporters of other non-fluorescent single-molecule species. A recent article reviews the active field of biolabeling in this perspective [8].

Nonetheless, since most applications of SMS in biochemistry and biology use fluorescent dyes as labels of proteins, DNA and RNA molecules, a simple model valid for single fluorescent dyes will be presented, allowing a presentation of the different parameters accessible with SMS.

4.2. Fluorescence emission

Fluorescence consists in the emission of a photon by a molecule returning from an excited electronic level to the ground state (singlet state S_0). Being spin-allowed, the transition is usually rapid, in the ns range (in contrast to phosphorescence, a process characterized by spin-forbidden, much slower de-excitation transitions [59]).

Excitation and emission processes are represented by a Jablonski diagram (Fig. 4(a)) depicting the initial, final and intermediate electronic and vibrational states of the molecule. Fast intramolecular vibrational relaxations result in emitted photons having a lower energy than the incident ones. This so-called Stokes shift allows a simple separation of the emitted fluorescence from the excitation light.

Upon excitation to the first excited state, the molecule has a certain probability to be shelved in a non-emitting triplet state from microseconds to milliseconds, resulting in 'dark' or off-states (Fig. 4, (b) and (c))
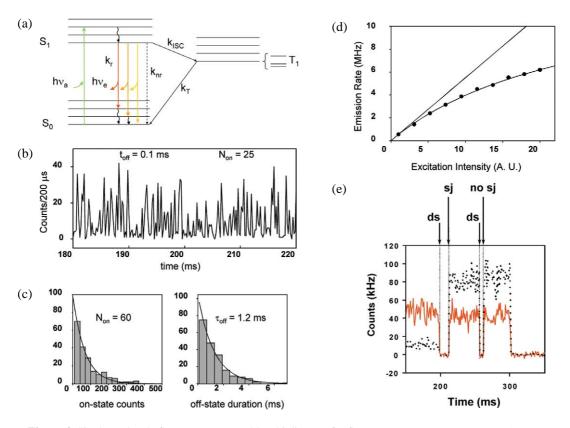
Figure 4. Single-molecule fluorescence. (a) Jablonski diagram for fluorescence (at room temperature). Upon absorption of a photon of energy $h\nu_a$ close to the resonance energy $E_{S_1} - E_{S_0}$, a molecule in a vibronic sublevel of the ground singlet state S_0 is promoted to a vibronic sublevel of the lowest excited singlet state S_1. Non-radiative, fast relaxation brings the molecule down to the lowest S_1 sublevel in picoseconds. Emission of a photon of energy $h\nu_e < h\nu_a$ (radiative rate k_r) can take place within nanoseconds and bring back the molecule to one of the vibronic sublevels of the ground state. Alternatively, collisional quenching may bring the molecule back to its ground state without photon emission (non-radiative rate k_{nr}). A third type of process present in organic dye molecules is intersystem crossing to the first excited triplet state T_1 (rate k_{ISC}). Relaxation from this excited state back to the ground state is spin-forbidden and thus the lifetime of this state is in the order of microseconds to milliseconds. Relaxation to the ground state takes place either by photon emission (phosphorescence) or non-radiative relaxation. The fluorescence lifetime is defined by $\tau = 1/\Gamma = (k_r + k_{nr})^{-1}$. (b) Fluorescence time trace (40 ms excerpt) of a Texas Red (TR) molecule attached to a 20-nucleotides long single-stranded DNA molecule immobilized on a silanized glass coverslip [71]. The confocal setup used is similar to the one depicted in Fig. 2. Excitation: CW 514 nm, circularly polarized, 6 kW/cm^2, binning: 200 μs. On- and off-states (the latter corresponding to the molecule being in the triplet state) alternate stochastically. (c) Histograms of on-state count (left) and off-state duration (right) for the time trace partially shown in (b). The decay parameters of the exponential fits (solid line) are indicated. $t_{off} = 1.2$ ms is the triplet state lifetime. $N_{on}^{-1} = k_{ISC} = 1.7\%$. (d) Intensity dependence of the emission rate of a single Texas Red molecule. The data departs from a linear dependence because of saturation due to intersystem crossing. The fitted curve yields a saturation rate of $R_S = 6.5$ MHz and a triplet lifetime $t_{off} = (k_{ISC} \cdot R_S)^{-1} = 10$ μs. The difference between this value and the value obtained in (c) illustrates the heterogeneity uncovered by single-molecule measurements. (e) Spectral jumps of a single Texas Red fluorophore attached to a single stranded DNA molecule [75]. Solid line: long wavelength channel, dotted line: short wavelength channel. ds: dark state, sj: spectral jump, no sj: dark state not followed by a spectral jump. Cases where spectral jumps are observed without noticeable dark states may still correspond to dark states with durations shorter than the time resolution of the experiment.
(a)–(c) *Adapted with permission from Ref.* [71]. *Copyright 1997, Elsevier Science B.V.* (e) *Adapted with permission from Ref.* [75]. *Copyright 1996, IEEE.*

[27,71,72]. This results in a saturation of the emitted count rate R (Fig. 4(d)) according to:

$$R = R_S \frac{I/I_S}{1 + I/I_S} \qquad (4)$$

where the saturation intensity is $I_S \sim 10$–100 kW/cm^2 and the saturation rate $R_S \sim 1$–20 MHz for typical fluorophores [59]. This puts a limit in *SNR* enhancement due to saturation of the emitted signal ('triplet bottleneck'). Other (if not all) fluorescent single molecules like GFP [63] or semiconductor nanocrystals [70,73,74] exhibit similar dark state intervals, although for different reasons (different long-lived dark states for GFP [63], Auger ionization or surface trapping of carriers for NCs [73]). Finally, spectral jumps can also be observed as illustrated in Fig. 2(e) [75]. This phenomenon results from a shift of absorption and emission maxima due to the changing environment of the molecule or a sudden conformational change of the molecule itself [30,31,76,77]. The corresponding changes in excitation and emission spectra are noticed by sudden fluctuations in the emitted intensity (due to wavelength dependence of the absorption cross section).

4.3. Fluorescence lifetime

A fluorescence photon is typically emitted within nanoseconds after absorption of the excitation photon. The decay law (or probability distribution of emission times) is usually mono-exponential, characterized by a lifetime $\tau = \Gamma^{-1} = (k_r + k_{nr})^{-1}$, where k_r and k_{nr} are the radiative and non-radiative decay rates respectively (Fig. 4(a)). However, the lifetime depends on the emission spectrum (which can change due to spectral shifts) and the local environment. For instance, the proximity to a dielectric or metallic surface markedly modifies the fluorescence lifetime via perturbations of the intramolecular transition matrix elements [43,76,78,79]. Fluorescence lifetime is in any case a sensitive probe of the environment of the molecule (Fig. 5). In addition, use of time-gated techniques to reject photons immediately after the excitation pulse is often a way to eliminate most of the background signal not rejected by filters (e.g. Raman scattering) [32].

Due to the ns-lifetime of most fluorophores, single-molecule lifetime measurements require using a pulsed laser source with picosecond or femtosecond pulse-width and time-correlated single-photon detection and analysis techniques. Once an expensive investment and a quite sophisticated technical challenge, the recent apparition of relatively inexpensive pulsed laser diodes and integrated electronics on a PC-board associated with software tools [45,80] will certainly extend its use in single-molecule analysis.

4.4. Fluorescence polarization

The efficiency of photon absorption by a fluorophore is proportional to $(\vec{E} \cdot \vec{\mu})^2$ where $\vec{E}$ represents the local electric field and $\vec{\mu}$ the absorption dipole moment of the fluorophore [59,81,82]. For a fixed fluorophore, recording the emitted fluorescence upon modulation of the excitation linear polarization allows the determination of the absorption dipole orientation (the emission dipole being generally nearly parallel to it). This information in turn allows the determination of the spatial orientation of the fluorophore [76, 77,83]. For a mobile molecule however, more information is needed, since the emission dipole may have time to tumble significantly during the few nanoseconds between absorption and emission [84]. The emission polarization is needed to fully recover the relevant information, as illustrated in Fig. 6. Different experimental schemes can be used, among which the near-field scheme (Fig. 3) and the confocal scheme (Fig. 2). In particular, it is important to recover the projection of the polarization on more than two orthogonal axes. This can be achieved in different ways in wide-field imaging approaches using TIR and taking advantage of aberrations induced by index mismatch in high numerical aperture objectives [85], defocalization effects [86] or excitation with alternating polarizations [82]. Other approaches using confocal scheme and using amplitude [87] or phase masks [88] allow a complete determination of this orientation.
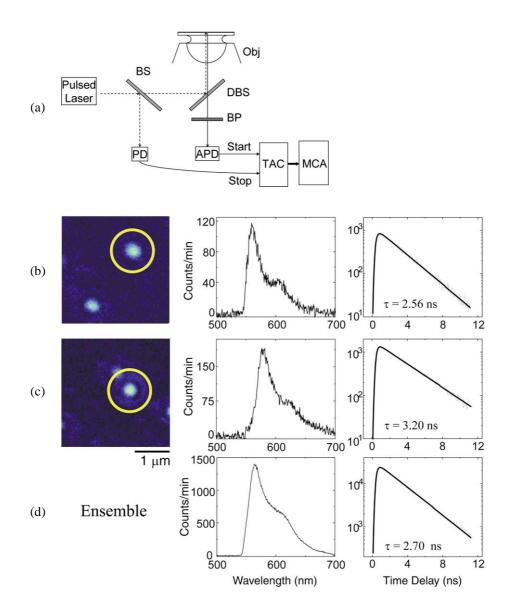
Figure 5. Lifetime measurements. (a) Schematic of a lifetime measurement setup. BS: beamsplitter used to deflect part of the incident pulse towards a fast photodiode (PD); DBS: dichroic beam splitter used to spectrally separate incident from emitted light; BP: band pass filter further rejecting stray light; APD: avalanche photodiode. For each detected photon, the APD emits a pulse, which is fed to the start input of a time-to-amplitude converter (TAC). A stop pulse from the laser immediately follows it (regularly emitted at a rate of τ_L^{-1}), allowing the measurement of the separation between both pulses. A multichannel analyzer (MCA) histograms the arrival times, resulting in the curves shown in the right part of (b)–(d). (b)–(d) Fluorescence images (left panels), corresponding spectra (middle), and fluorescence decays (right) for two molecules located at a PMMA–air interface. The peak emission wavelength λ_p was 560 nm in (b) and 578 nm in (c). Lifetimes were fit to a single exponential (dotted curves), with decay times of $\tau = 2.56$ ns (b) and 3.20 ns (c). An ensemble measurement of spectrum and fluorescence decay averaged over several hundred of molecules is shown in (d). The ensemble values are $\lambda_p = 565$ nm and $\tau = 2.70$ ns.
(b)–(d) *Adapted from Ref.* [43]. *Copyright 1996, the American Association for the Advancement of Science.*
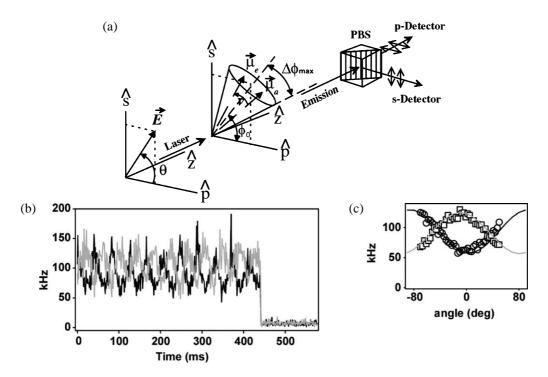
Figure 6. Polarization measurements. (a) Experiment schematic. $\vec{E}$: electric field, making an angle θ with the p polarization axis. The excitation propagates along axis z, which is also the collection axis. $\vec{\mu_a}$ and $\vec{\mu_e}$ are the absorption and emission dipole moments, initially aligned. ν represents the rotational diffusion of the emission dipole during the excited lifetime. The dipole is supposed to be confined in a cone positioned at an angle ϕ_0 projected on the (s, p) plane, and having a half-angle $\Delta\phi_{max}$. A polarizing beam-splitter (PBS) splits the collected emission in two signals I_s and I_p, which are simultaneously recorded by APDs. (b) Simultaneously recorded I_s (black) and I_p (gray) of a molecule rapidly rotating in liquid. (c) Same data as in (b), but average over the 11 'on' periods. The fit corresponds to a $\Delta\phi_{max}$ close to 90° (freely rotating molecule) and permits determination of the constrained rotational diffusion parameter.
(a)–(c) *Adapted with permission from Ref.* [84]. *Copyright 1998, the American Physical Society.*

In the case of a planar degenerate transition dipole as exhibited by nanocrystals or some highly symmetric molecules, a simpler approach using variable polarization excitation provides the 3-dimensional orientation of the molecule [48].
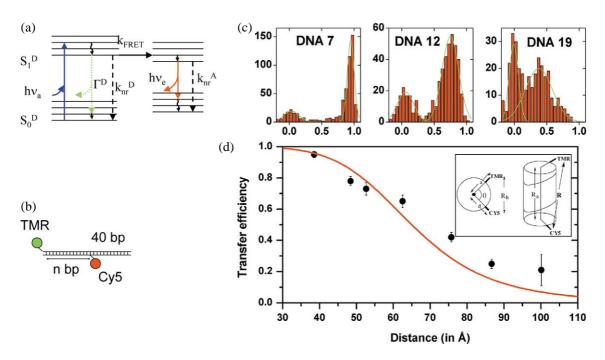
4.5. Fluorescence resonance energy transfer

A special case of local influence of the environment on fluorescence is encountered in fluorescence resonance energy transfer (FRET, see Fig. 7(a)), first described theoretically by Förster in 1947 [59,89,90]. In case of the presence of a nearby (acceptor) molecule having an absorption spectrum overlapping the donor emission spectrum, part of the energy absorbed by the donor is transferred non-radiatively to the acceptor with an efficiency E given by:

$$E = \left(1 + \left(\frac{r}{R_0}\right)^6\right)^{-1},$$

(5)

where r is the distance between the two emitting centers and R_0 is the Förster radius (in Å):

$$R_0 = a\left(\kappa^2 n^{-4} Q_D J(\lambda)\right)^{1/6}.$$

(6)

631

Figure 7. Single pair fluorescence resonance energy transfer. (a) Jablonski diagram for FRET. Fluorescence energy transfer involves two molecules: a donor D and an acceptor A whose absorption spectrum overlaps the emission spectrum of the donor. Excitation of the acceptor to the lowest singlet excited state is a process identical as that described for single-molecule fluorescence (Fig. 2(d)). In the presence (within a few nm) of a nearby acceptor molecule, donor fluorescence emission is largely quenched by energy transfer to the acceptor by dipole–dipole interaction. The donor exhibits fluorescent emission following the rules outlined in Fig. 2(d). (b) DNA n constructs used for the FRET distance study. Tetramethylrhodamine (TMR) is attached to the $5'$ end of the DNA and Cy5 is attached to the nth base from the end ($n = 7, 12, 14, 16, 19, 24$ and 27). (c) FRET histograms extracted from time traces for DNAs 7, 12, and 19, as shown in Fig. 2(b). Double Gaussian fits extract numbers for the mean (width) of the higher efficiency peak of 0.95 ± 0.05, 0.75 ± 0.13, and 0.38 ± 0.21, respectively. The peak around zero efficiency corresponds to bleached or inactive acceptor molecules. (d) Mean FRET efficiencies extracted from FRET histograms plotted as a function of distance for DNA 7, 12, 14, 16, 19, 24, and 27. Distances are calculated using the known B-DNA double helix structure. The solid line corresponds to the expected Förster transfer curve with $R_0 = 65$ Å. (b)–(c) *Adapted with permission from Ref.* [44]. *Copyright 1999, the National Academy of Sciences USA.*

In this complex expression, $a = 9.78 \cdot 10^3$, n is the refractive index of the medium, Q_D the donor fluorescence quantum yield in the absence of the acceptor and $J(\lambda)$ is a spectral overlap integral (in $M^{-1} \cdot cm^3$). κ^2 is a geometric factor, which averages out to $2/3$ in the case of freely rotating dyes. Typical order of magnitude for R_0 is a few nanometers, which sets the range of distances within which this effect is measurable. FRET is thus very sensitive to the donor–acceptor distance, which makes it a useful molecular ruler [91]. Experimentally, the efficiency is measured as a function of the recorded donor (F_D) and acceptor (F_A) emissions (dual-channel measurement) via:

$$E = \left(1 + \alpha \frac{F_D}{F_A} \frac{Q_A}{Q_D}\right)^{-1}, \tag{7}$$

where Q_A and Q_D are the fluorescence quantum yields of the donor and acceptor, respectively, and α is a correction factor accounting for the different channel detection efficiencies. An illustration of this utilization is given in Fig. 7, (b)–(d), where different predefined distances between donor and acceptors are

set by rigid double-stranded DNA molecules [44]. The corresponding donor–acceptor distances are readily measured on diffusing molecules, with subnanometer precision.

Alternatively, the transfer efficiency can be measured via the fluorescence lifetimes as

$$E = 1 - \frac{\tau_{D(A)}}{\tau_{D(0)}}, \tag{8}$$

where $\tau_{D(A)}$ and $\tau_{D(0)}$ are the donor lifetimes in the presence or absence of acceptor, respectively [92].

4.6. Other spectroscopies

Although most single-molecule experiments use one-photon fluorescence excitation because of its relatively large cross section ($\sim 10^{-16}$ cm^2), other types of spectroscopic techniques can be used at the single-molecule level. Fluorescence can for instance be excited via a two-photon absorption process, whereby a laser excitation with half the photon energy needed to attain the excited state is used [93]. However, due to the very low cross section (e.g. $37 \cdot 10^{-50}$ cm$^2 \cdot$s$\cdot$photon^{-1} at 780 nm for FITC [94]) and the quadratic dependence in the incident power (two simultaneous photons are needed for excitation), an excitation power several orders of magnitude larger than for one-photon excitation is needed. In compensation, excitation takes place in a substantially reduced volume of the sample, reducing the out-of-focus background contribution and bleaching. However, the higher power required increases the probability of photobleaching due to the increased probability of photochemical degradation in the long-lived triplet state and the interplay of multi-photon ionization processes [95].

Although Raman scattering cross sections ($\sim 10^{-30}$ cm^2) are orders of magnitude lower than fluorescence absorption cross section, they can be enormously amplified if the single molecule is trapped in a so-called 'hot spot' of a metallic nanoparticle, giving rise to surface-enhanced Raman scattering (SERS) [96]. Highly resolved vibrational information can be recovered, exhibiting much more stable emission than fluorescence. Moreover, this technique can be applied to non-fluorescent molecules. Similarly to fluorescence, the technique can be extended to non-linear (two-photon) regimes, as in surface-enhanced hyper-Raman scattering and surface-enhanced anti-Stokes Raman scattering [97]. However, since they require the single molecule to be located on rare sites of a metallic particle, these methods have only been applied to fundamental chemical studies of molecular species.

Finally, electron transfer can significantly perturb the lifetime of a dye by opening a new non-radiative path in the Jablonski diagram of the molecule (Fig. 4(a)). It was first demonstrated at the single-molecule level in a dye-photosensitization system inspired by chemical solar-cell science [98] but has the potential to become a powerful molecular ruler at the angström level in chemistry and biochemistry [99].

4.7. High-resolution localization

High-resolution localization of nanometer-sized objects (nanogold particles [100] or motor proteins coupled to micrometer-sized latex beads [101]) with light-microscopy was first made possible by digitally-enhanced video recording. Nanometer-resolution localization of the center of mass of these objects is simply obtained by fitting the expected microscopic image to the observed one or by simple centroid-finding algorithms [102]. Both methods rely on the good *SNR* that can be obtained at video-rate in these high-contrast bright-field images. In fluorescence microscopy, the image of an emitting object of dimension smaller that the emission wavelength (point-like object) is identical to the response function of the microscope (or point-spread function, PSF), typically close to an Airy function with micrometer dimension [103]. As in bright-field microscopy, localization of point-like fluorescent sources can likewise be achieved with nanometer-resolution in three dimensions provided the *SNR* is large enough [104]. Extension of the previous approaches to single fluorescent molecules had to await improvements in sensitivity allowing acquisition of images with good *SNR* before photobleaching of the molecule occurred.
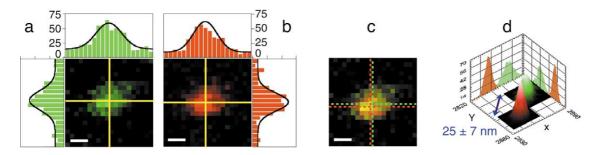
Figure 8. Semiconductor nanocrystal colocalization. (a), (b) Mixture of green (Em: 540 nm) and red (Em: 620 nm) NCs excited at 488 nm (excitation power: 200 nW incident or 320 W/cm^2 peak irradiance, integration time: 50 ms/pixel) and imaged in a custom-made confocal microscope using APD detection (see Ref. [108] for details). Green and red channel images of a 1×1 μm^2 scan (pixel size: 50 nm, scale bar: 200 nm). The yellow crosses indicate the fitted PSF centers. The image intensity profiles along the two lines are represented as bar graphs; the black curve corresponds to the 2D elliptical Gaussian fit. (c) Overlay of the two channels. The green and red dashed crosses indicate the centers of the green and red PSFs, respectively. (d) Histograms of the fitted centers distribution of 1000 bootstrap simulations of each channel. Each probability distribution has a width of a few nanometers, corresponding to the uncertainty of the nanocrystal positions. Coordinates indicate absolute position (in nm) of the closed-loop piezo-scanner. These probability distributions are well fitted by 2D tilted Gaussians. The measured distance is 25 ± 7 nm.
(a)–(d) *From Ref.* [108]. *Copyright 2001, Academic Press.*

Although single-molecule imaging was first achieved using NSOM (Fig. 3) [28], scanning (Fig. 5) [43] and non scanning far-field approaches [33] offer several advantages among which ease of use stands first. High-resolution localization of fluorescent molecules by PSF fitting works, however, as long as individual molecules are well separated. It fails for distances slightly smaller than that given by the Rayleigh criterion [105], due to the overlap of the individual molecules' PSFs. Two direct strategies have been proposed to go beyond this limit: one is based on using different spectral characteristics to distinguish between nearby molecules [46,47,75,106], the other is based on reducing the size of the PSF in two or more dimensions [107]. For instance, Fig. 8 presents an example of nanometer-resolution colocalization of closely spaced semiconductor nanocrystals, relying on their property of being excitable with a single excitation wavelength, while emitting at a size-dependent wavelength [108].

5. Applications of single-molecule spectroscopy

Single-molecule methods are now used in several domains. Due to their very rapid adaptation by many researchers, we will not attempt to review their applications exhaustively but instead present few illustrative examples chosen in different fields.

5.1. Molecular physics

The realization that the fluorescence of a single molecule could be detected with a good *SNR* over extended periods of time, especially embedded in a crystalline matrix at cryogenic temperature, has led to high-resolution experiments aimed at determining molecular energy levels and transitions [1,2,14]. In particular, studies of transitions between sublevels of the triplet state by electron spin resonance (ESR) using superimposed radio-frequency pulses have permitted a precise test of the quantum description of such systems [10,109,110]. The DC and AC Stark effect (shift of a transition energy in the presence of a fixed or alternating electric field) has also been studied in several systems, allowing the symmetry and deformations of the molecule to be determined [10,111]. Similar approaches have been used to study the photophysics of luminescent polymers (J-aggregates) [112], light-harvesting complexes [113], green fluorescent proteins (GFP) [63] or semiconductor nanocrystals [70] and other systems. In addition to providing direct tests

for theoretical models, these fundamental studies turn out to be crucial to understand the behavior of single molecules in complex environments. Finally, reliable observation and control of single molecules is a prerequisite of the full development of nanotechnology and quantum computing and communication using single-photon sources [9].

5.2. Material science studies

Single-molecule photophysical properties are extremely sensitive to their local (nanometer-sized) environment [1,2]. They can for instance report on parameters like the local pH [114], or on the local structure as illustrated by experiments designed to study the local dynamics of a polymer matrix at the onset of the glass transition (Fig. 9) [4].

In this experiment, molecules of the organic fluorophore rhodamine 6G (R6G) dispersed within a thin poly(methacrylate) film (250 nm) were observed at temperatures slightly above the melting temperature of the polymer, using a confocal microscope detecting the s and p polarization of the emitted fluorescence (Fig. 6(a)). Observations were performed under nitrogen atmosphere and at low excitation power (20 nW) in order to prevent oxidation, thus allowing long observation time (several hours). Each observed R6G molecule exhibited a slow rotational diffusion, sometimes accompanied by lateral or transverse diffusion on a much longer time scale (Fig. 9(a)). Computation of the autocorrelation function of the emission polarization shows a multi-exponential decay, pointing to a distribution of time scales of rotational diffusion. A closer look at sub-windows of the time trace reveals however that the decay comes closer to a mono-exponential behavior at shorter time scales (Fig. 9, (b) and (c)). This study demonstrates that an individual molecule probes an increasing number of different environments over time (dynamic disorder). At long time scales, the observable characteristics (such as the autocorrelation function) are similar to those measured on ensemble of molecules, as expected from the ergodicity hypothesis. At short time scale, each molecule reveals the peculiar local and stable characteristic of its nano-environment, which may be different from that of another molecule situated elsewhere (static disorder).

5.3. Biophysical and biological studies

SMS has allowed a reassessment of long-standing questions in biophysics, biochemistry and biology [5,7], by giving scientists the possibility to look at and study conformational dynamics and interactions of individual molecule in biological processes [54]. From simple model systems based on DNA [81, 84] or small peptides [115], the complexity of the systems studied has raised to ribozyme [116], motor-proteins [117,118] and other biomolecules [119] or biomolecular complexes formed by association of a few molecules [120].

To simplify the task, some biological molecules are intrinsically fluorescent because of tryptophan residues, or because they bind cofactors which are fluorescent in one of their oxidation state (e.g. nicotinamide adenine dinucleotide (NADH) emits at 460 nm, flavin adenine dinucleotide (FAD) at 525 nm). For instance, the cholesterol oxidase (CO_x) enzyme of *Brevibacterium* sp., an enzyme that catalyzes the oxidation of cholesterol by oxygen, uses FAD as a cofactor. As a result, one can study the dynamics of this enzyme at the single-molecule level by monitoring the fluorescence of its active site. The experiment presented in Fig. 10 uses a confocal setup with enzymes immobilized in an agarose gel. The intervals during which the enzyme is active ('on' states) are followed by intervals during which it is inactive ('off' states). The fluorescence recording of a single enzyme thus appears as a blinking time trace, as shown in Fig. 10(b). Relevant kinetic parameters can be extracted from the distribution of on and off times. In addition to revealing heterogeneity between enzymes of the same batch characterized by different kinetic parameters for the catalysis reaction (static disorder), this experiment reveals a dynamic heterogeneity or 'memory effect' for each individually studied enzyme. Specifically, one observes a tendency for short on times to follow short on times, and for long on times to follow long on times (Fig. 10(c)). The characteristic time scale of this correlation is comparable to that observed for spectral fluctuations of the emission spectrum,
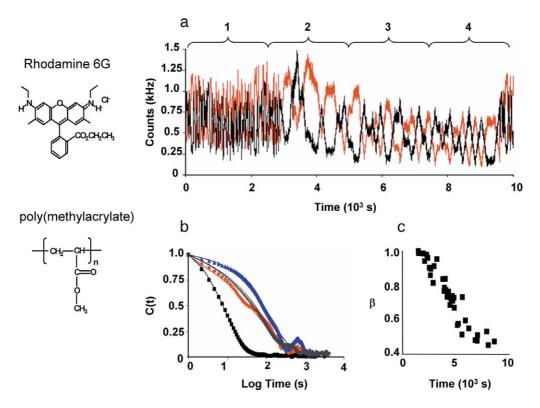
Figure 9. Polymer dynamics near the glass transition. (a) Fluorescence intensity of a single long-lived rhodamine 6G molecule in poly(methylacrylate) (PMA) at 291 K detected at orthogonal polarizations (red: s and black: p polarizations). The melting temperature of PMA is $T_g = 281$ K. The time trace integration is 1 s. This time trace shows the anticorrelation of both polarizations, characteristic of a rotational diffusion of the molecule. Different regimes are observed along the time trace (1–4), which could be due either to a modification of the local 'cage' in which the molecule rotates, or escape of the molecule to another nearby nano-environment. The autocorrelation function of polarization computed over the whole trace (not shown) is well fitted by a model adapted to the non-exponential relaxation of polymers, the Kohlrausch–Williams–Watt (*KWW*) model:

$$KWW(t) \propto e^{-(t/\tau)^\beta}$$

with $\tau = 88$ s, $\beta = 0.46$. (b) Correlation functions of subsets 1–4 of the full trace. 1 (black squares): $\tau = 15$ s, $\beta = 1.0$. 2 (blue triangles): $\tau = 112$ s, $\beta = 0.77$. 3 (open circles): $\tau = 90$ s, $\beta = 0.59$. 4 (red diamonds): $\tau = 64$ s, $\beta = 0.59$. The β exponent is closer to 1, showing that the rotational diffusion is an unhindered one at short time scales, converging to the bulk exponent at larger time scale due to ergodicity. This experiment illustrates changes of environment as the observed molecule diffuses and rotates through the polymer mesh, changes that are hidden in ensemble measurements. (c) Values of β as a function of photochemical survival time in PMA at $T_g + 5$ K. (a)–(c) *Adapted with permission from Ref.* [4]. *Copyright 2001, The American Association for the Advancement of Science.*

pointing to slow conformational fluctuations as the origin of this phenomenon. This observation of both static and dynamic disorder in a single enzyme behavior is reminiscent of that of rhodamine 6G molecules in a polymer matrix (Section 5.2). Although of different origin in these two experiments, both effects can be studied easily by similar single-molecule techniques.

Few biological molecules, however, have a sufficient intrinsic fluorescence to be studied with single-molecule sensitivity. To study non-fluorescent molecules, several labeling schemes exist, which allow quantitative, site-specific labeling of proteins, nucleic acid or lipid molecules without compromising
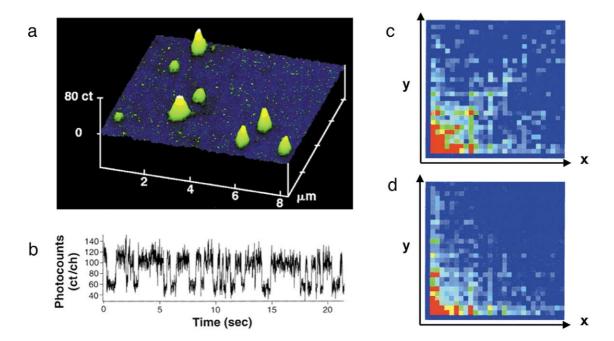
Figure 10. Single enzyme dynamics. (a) Fluorescence image of single cholesterol oxidase (Cox) molecules immobilized in a 10-μm-thick film of agarose gel of 99% pH 7.4 buffer solution (8 μm by 8 μm, 4 min scan, 500 nW excitation at 442 nm). The emission is from the fluorescent active site, FAD, which is tightly bound to the center of CO_x. Each individual peak is attributed to a single CO_x molecule. The intensity variation between the molecules is due to different longitudinal positions in the light depths. (b) Real-time observation of enzymatic turnovers of a single CO_x molecule catalyzing oxidation of cholesterol molecules. This panel shows a portion of an emission intensity trajectory recorded in 13.1 ms per channel. The trajectory was recorded with a cholesterol concentration of 0.2 mM and saturated oxygen concentration of 0.25 mM. The emission exhibits stochastic blinking behavior as the FAD toggles between oxidized (fluorescent) and reduced (nonfluorescent) states, each on-off cycle corresponding to an enzymatic turnover. More than 500 on-off cycles are recorded in this trajectory. (c) The 2D conditional probability distribution for on-times (x and y) of two adjacent turnovers as derived from the trajectories of 33 CO_x molecules with 2 mM 5-pregene-3-20-diol substrate, a derivative of cholesterol. The scale of x- and y-axes are from 0 to 1 s. A subtle diagonal feature is present, indicative of a memory effect. (d) The 2D conditional histogram for two on-times separated by 10 turnovers for the CO_x molecules in (c). The diagonal feature vanishes because the two on-times become independent of each other at the 10-turnover separation. The color code in (c) and (d) represents the occurrence (z axis) from 350 (red) to 0 (purple).
(a)–(d) *Adapted with permission from Ref.* [64]. *Copyright 1998, The American Association for the Advancement of Science.*

their functionality. They range from in vitro techniques of site-specific labeling or unnatural amino-acid insertion, to in vivo techniques involving genetic engineering of GFP-tagged proteins [8,59].

An example of this versatility is provided by the labeling of the central part of a rotary motor protein, F_1-ATPase [119]. In this experiment, the molecular rotor was labeled with a single fluorophore whose orientation, detected by emission polarization measurements, directly reported the angle of the rotor with respect to the shaft. The small size of the fluorophore guaranteed that the protein motion would not be hindered, contrary to previous experiments, which used much larger reporters (micron size latex beads or fluorescent actin filaments). This experiment reproduced the previous results, showing that the rotor performed 120° steps (more recent work revealed substeps of 90° and 30° [121]).

One of the domains where SMS can be of great importance is the study of protein folding that still lacks a comprehensive theoretical treatment [6]. The transition from a denatured state to the fully folded
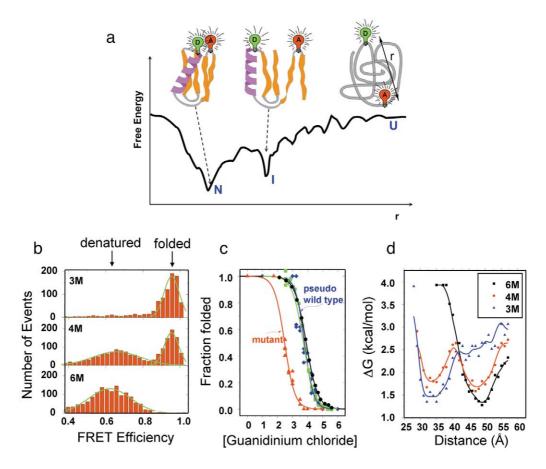
Figure 11. Protein folding. (a) Energy landscape for a protein folding reaction represented as a cartoon of the free energy as function of distance r between donor and acceptor. The rugged energy landscape has a funnel shape with three extrema: U (unfolded state), I (intermediate state) and N (folded or native state). In this labeling scheme, donor and acceptor are close to one another in the native, folded state (N), resulting in a high FRET efficiency. There is reduced energy transfer (larger distance) in the denatured, unfolded state (U). (b) Single-molecule protein folding data. Single pair FRET (spFRET) histograms of the pseudo wild type enzyme chymotrypsin inhibitor 2 (PWT CI2) at 3, 4, and 6M denaturant (guanidinium chloride). The FRET efficiency exhibits two peaks, one for folded molecules (high FRET) and one for unfolded molecules (low FRET). Population is transferred from folded to unfolded at higher denaturant concentration, as expected from the protein labeling schematically depicted in (a). (c) Ensemble and single-molecule denaturation curves for PWT and K17G mutant CI2. Symbols correspond to data, lines showing sigmoidal fits. PWT CI2: ensemble tryptophan fluorescence experiment (black circles), ensemble FRET (green squares), spFRET (blue diamonds); K17G mutant CI2 spFRET (red triangles). (d) Free energy functions for PWT CI2 at 3, 4, and 6M denaturant. The solid lines represent a smoothing of the data and are only meant to guide the eye. (a) *Adapted with permission from Ref.* [6]. *Copyright 2000 Nature Structural Biology.* (b)–(d) *Adapted with permission from Ref.* [122]. *Copyright 2000, The National Academy of Sciences.*

native protein usually involves an unknown number of intermediate states, which are not accessible by ensemble measurements. Conformations of doubly labeled proteins can be monitored by SMS as they undergo folding, taking advantage of the distance dependence of FRET (demonstrated for a model DNA system in Section 4.5, Fig. 7). Fig. 11 shows one of many examples of such a study, performed on diffusing molecules in solution, a configuration that suppresses uncontrolled effects of nearby surfaces. The enzyme chymotrypsin inhibitor 2 (CI2) is a model system for protein folding, believed to have two clearly distinct folding states, which can be controlled by the concentration of denaturant guanidinium

chloride [122]. Using single-pair FRET (spFRET) techniques, it is possible identify folded and unfolded molecules present at different denaturant concentration (Fig. 11(b)). When averaged, these measurements yield the same denaturation curve as obtained by ensemble measurements (Fig. 11(b)) and give access to the energy landscape of the folding reaction. The additional information provided by spFRET is the number of molecules in the two different states, providing direct evidence of the two states model derived indirectly from ensemble measurements.

Other biological systems have been successfully studied using the spFRET approach on immobilized molecules. In this experimental configuration, intramolecular spFRET (used in the CI2 study) allows monitoring conformational changes in real time. For instance, spFRET has revealed transient intermediate states in the *Tetrahymena* ribozyme [116], which had remained unnoticed in ensemble studies. In vivo, intermolecular spFRET permits the detection of association and dissociation events, as in the case of a epidermal growth factor receptor pair studied on cell membrane using TIR [123]. For cluster formation involving larger numbers of monomers, observed for instance with E-cadherin [124] or L-type Ca^{2+} channels [125], stoichiometric approaches relying on the quantized emission of single molecules can estimate the number of components in an aggregate.

6. Perspectives

SMS is now a mature discipline, allowing researchers to go beyond a mere verification of established results and address unsolved questions. It will doubtless be useful in domains beyond those mentioned in this article. Its ease of implementation will entice more scientists of other disciplines to utilize its methodology, each having specific goals in mind that are difficult to foresee.

The principle limitations of SMS outlined in Section 3 (low signal, limited life span of fluorophores, trade-off between time resolution and the level of detail of information) will remain, but technical improvements, especially towards simultaneous acquisition of all the fluorescence parameters described in Section 4 (spectrum, lifetime, polarization) are promising. In particular it is expected that new detectors will permit the combination of the high time resolution of single-photon counting devices with the large field of view and spectral resolution allowed by 2-dimensional detectors.

As powerful at it may be, SMS cannot replace every existing single-molecule detection or manipulation technique. It will most likely be associated with other approaches to correlate applied forces or fields and molecular conformations. New ways of controlling local fields (electric, magnetic or others) or biochemical environments (microfluidic devices) would take advantage of the non-invasiveness, high-temporal and spatial resolution of SMS to get a direct feedback of events at the nanometer scale and follow live processes in individual cells [126,127].

References

[1] W.E. Moerner, Examining nanoenvironments in solids on the scale of a single, isolated impurity molecule, Science 265 (1994) 46–53.

[2] W.E. Moerner, M. Orrit, Illuminating single molecules in condensed matter, Science 283 (1999) 1670–1676.

[3] D.S. English, E.J. Harbron, P.F. Barbara, Role of rare sites in single molecule spectroscopy measurements of spectral diffusion, J. Chem. Phys. 114 (2001) 10479–10485.

[4] L.A. Deschenes, D.A. Vanden Bout, Single-molecule studies of heterogeneous dynamics in polymer melts near the glass transition, Science 292 (2001) 255–258.

[5] S. Weiss, Fluorescence spectroscopy of single biomolecules, Science 283 (1999) 1676–1683.

[6] S. Weiss, Measuring conformational dynamics of biomolecules by single molecule fluorescence spectroscopy, Nature Struct. Biol. 7 (2000) 724–729.

[7] A. Ishijima, T. Yanagida, Single molecule nanobioscience, Trends Biochem. Sci. 26 (2001) 438–444.

[8] A. Kapanidis, S. Weiss, Fluorescent probes and bioconjugation chemistries for single-molecule fluorescence analysis of biomolecules, J. Chem. Phys. (2002), to be published.

[9] B. Lounis, W.E. Moerner, Single photons on demand from a single molecule at room temperature, Nature 407 (2000) 491–493.

[10] T. Basché, W.E. Moerner, M. Orrit, U.P. Wild (Eds.), Single-Molecule Optical Detection, Imaging and Spectroscopy, VCH, Weinheim, 1997.

[11] S. Nie, R.N. Zare, Optical detection of single molecules, Annu. Rev. Biophys. Biomol. Struct. 26 (1997) 567–596.

[12] T. Plakhotnik, E.A. Donley, U.P. Wild, Single molecule spectroscopy, Annu. Rev. Phys. Chem. 48 (1997) 181–212.

[13] X.S. Xie, J.K. Trautman, Optical studies of single molecules at room temperature, Annu. Rev. Phys. Chem. 49 (1998) 441–480.

[14] P. Tamarat, A. Maali, B. Lounis, M. Orrit, Ten years of single-molecule spectroscopy, J. Phys. Chem. A 104 (2000) 1–16.

[15] R. Rigler, E.S. Elson (Eds.), Fluorescence Correlation Spectroscopy. Theory and Applications, Springer, 2001.

[16] R. Rigler, M. Orrit, T. Basche (Eds.), Single Molecule Spectroscopy, Springer-Verlag, Stockholm, 2001.

[17] J. Perrin, La fluorescence, Ann. Phys. 10 (1918) 133–159.

[18] A. Lewis, A. Isaacson, A. Harootunian, A. Muray, Development of a 500 Å spatial resolution light microscope. I. Light is efficiently transmitted through λ/16 diameter apertures, Ultramicroscopy 13 (1984) 227–230.

[19] D.W. Pohl, W. Denk, M. Lanz, Optical stethoscopy: Image recording with resolution λ/20, Appl. Phys. Lett. 42 (1984) 651–653.

[20] E. Betzig, J.K. Trautman, Near-field optics: Microscopy, spectroscopy, and surface modification beyond the diffraction limit, Science 257 (1992) 189–195.

[21] E. Neher, B. Sakmann, Single-channel currents recorded from membrane of denervated frog muscle fibres, Nature 260 (1976) 799–802.

[22] G. Binning, H. Rohrer, C. Gerber, E. Weibel, Surface studies by scanning tunneling microscopy, Phys. Rev. Lett. 49 (1982) 57–61.

[23] G. Binning, C.F. Quate, C. Gerber, Atomic force microscope, Phys. Rev. Lett. 56 (1986) 930–933.

[24] B.L. Blackford, M.H. Jericho, P.J. Mulhern, A review of tunneling microscope and atomic force microscope imaging of large biological structures – Problem and prospects, Scanning Microscopy 5 (1991) 907–918.

[25] H.G. Hansma, K.J. Kim, R.A. Garcia, M. Argaman, M.J. Allen, S.M. Parsons, Properties of biomolecules measured from atomic force microscope images: A review, J. Struct. Biol. 119 (1997) 99–108.

[26] W.E. Moerner, L. Kador, Optical detection and spectroscopy of single molecules in a solid, Phys. Rev. Lett. 62 (1989) 2535–2538.

[27] M. Orrit, J. Bernard, Single pentacene molecules detected by fluorescence excitation in a *p*-terphenyl crystal, Phys. Rev. Lett. 65 (1990) 2716–2719.

[28] E. Betzig, R.J. Chichester, Single molecules observed by near-field scanning optical microscopy, Science 262 (1993) 1422–1425.

[29] T. Basché, W.E. Moerner, Optical modification of a single impurity molecule in a solid, Nature 355 (1992) 335–337.

[30] J.K. Trautman, J.J. Macklin, L.E. Brus, E. Betzig, Near-field spectroscopy of single molecules at room temperature, Science 369 (1994) 40–42.

[31] W.P. Ambrose, W.E. Moerner, Fluorescence spectroscopy and spectral diffusion of single impurity molecules in a crystal, Nature 349 (1991) 225–227.

[32] E.B. Shera, N.K. Seitzinger, L.M. Davis, R.A. Keller, S.A. Soper, Detection of single fluorescent molecules, Chem. Phys. Lett. 174 (1990) 553–557.

[33] T. Schmidt, G.J. Schütz, W. Baumgartner, H.J. Gruber, H. Schindler, Imaging of single molecule diffusion, Proc. Nat. Acad. Sci. USA 93 (1996) 2926–2929.

[34] G.J. Schütz, V.P. Pastushenko, H. Gruber, H.-G. Knaus, B. Pragl, H. Schindler, 3D Imaging of individual ion channels in live cells at 40 nm resolution, Single Molecules 1 (2000) 25–31.

[35] Y. Sako, K. Hibino, T. Miyauchi, Y. Miyamoto, M. Ueda, T. Yanagida, Single-molecule imaging of signaling molecules in living cells, Single Molecules 1 (2000) 159–163.

[36] L. Fleury, B. Sick, G. Zumofen, B. Hecht, U.P. Wild, High photo-stability of single molecules in an organic crystal at room temperature observed by scanning confocal microscopy, Mol. Phys. 95 (1998) 1333–1338.

[37] F. Kulzer, F. Koberling, T. Christ, A. Mews, T. Basché, Terrylene in *p*-terphenyl: single-molecule experiments at room temperature, Chem. Phys. 247 (1999) 23–34.

[38] T. Hirschfeld, Optical microscopic observation of single small molecules, Appl. Opt. 15 (1976) 2965–2966.

[39] D.C. Nguyen, R.A. Keller, H. Jett, J.C. Martin, Detection of single molecules of phycoerythrin in hydrodynamically focused flows by laser-induced fluorescence, Anal. Chem. 59 (1987) 2158–2161.

[40] S. Nie, D.T. Chiu, R.N. Zare, Probing individual molecules with confocal fluorescence microscopy, Science 266 (1994) 1018–1021.

[41] J. Widengren, R. Rigler, Fluorescence correlation spectroscopy as a tool to investigate chemical reactions in solutions and on cell surfaces, Cell. Mol. Biol. 44 (1998) 857–879.

[42] P. Schwille, Fluorescence correlation spectroscopy and its potential for intracellular applications, Cell Biochem. Biophys. 34 (2001) 383–408.

[43] J.J. Macklin, J.K. Trautman, T.D. Harris, L.E. Brus, Imaging and time-resolved spectroscopy of single molecules at an interface, Science 272 (1996) 255–258.

[44] A.A. Deniz, M. Dahan, J.R. Grunwell, T. Ha, A.E. Faulhaber, D.S. Chemla, S. Weiss, P.G. Schultz, Single-pair fluorescence energy transfer on freely diffusing molecules: Observation of Förster distance dependence and subpopulations, Proc. Nat. Acad. Sci. USA 96 (1999) 3670–3675.

[45] P. Tinnefeld, V. Buschmann, D.-P. Herten, K.-T. Han, M. Sauer, Confocal fluorescence lifetime imaging microscopy (flim) at the single molecule level, Single Molecules 1 (2000) 215–223.

[46] A.M. van Oijen, J. Köhler, J. Schmidt, M. Müller, G.J. Brakenhoff, 3-dimensional super-resolution by spectrally selective imaging, Chem. Phys. Lett. 292 (1998) 183–187.

[47] T.D. Lacoste, X. Michalet, F. Pinaud, D.S. Chemla, A.P. Alivisatos, S. Weiss, Ultrahigh-resolution multicolor colocalization of single fluorescent probes, Proc. Nat. Acad. Sci. USA 97 (2000) 9461–9466.

[48] S.A. Empedocles, R. Neuhauser, M.G. Bawendi, Three-dimensional orientation measurements of symmetric single chromophores using polarization microscopy, Nature 399 (1999) 126–130.

[49] M. Nirmal, B.O. Dabbousi, M.G. Bawendi, J.J. Macklin, J.K. Trautman, T.D. Harris, L.E. Brus, Fluorescence intermittency in single cadmium selenide nanocrystals, Nature 383 (1996) 802–804.

[50] R.G. Neuhauser, K.T. Shimizu, W.K. Woo, A.S. Empedocles, M.G. Bawendi, Correlation between fluorescence intermittency and spectral diffusion in single semiconductor quantum dots, Phys. Rev. Lett. 85 (2000) 3301–3304.

[51] T. Basché, W.E. Moerner, M. Orrit, H. Talon, Photon antibunching in the fluorescence of a single dye molecule trapped in a solid, Phys. Rev. Lett. 69 (1992) 1516–1519.

[52] J.B. Pawley (Ed.), Handbook of Biological Confocal Microscopy, Plenum Press, New York, 1995.

[53] M. Goulian, S.M. Simon, Tracking single proteins within cells, Biophys. J. 79 (2000) 2188–2198.

[54] T. Funatsu, Y. Harada, M. Tokunaga, K. Saito, T. Yanagida, Imaging of single fluorescent molecules and individual ATP turnovers by single myosin molecules in aqueous solution, Nature 374 (1995) 555–559.

[55] M.F. Paige, E.J. Bjernfeld, W.E. Moerner, A comparison of through-the-objective total internal reflection microscopy and epifluorescence microscopy for single-molecule fluorescence imaging, Single Molecules 2 (2001) 191–201.

[56] H. Kume, K. Koyama, K. Nakatsugawa, S. Suzuki, D. Fatlowitz, Ultrafast microchannel plate photomultipliers, Appl. Opt. 27 (1988) 1170–1178.

[57] H. Dautet, P. Deschamps, B. Dion, A.D. MacGregor, D. MacSween, R.J. McIntyre, C. Trottier, P.P. Webb, Photon counting techniques with silicon avalanche photodiodes, Appl. Opt. 32 (1993) 3894–3900.

[58] A. Spinelli, L.M. Davis, H. Dautet, Actively quenched single-photon avalanche diode for high-repetition rate time-gated photon counting, Rev. Sci. Instrum. 67 (1996) 55–61.

[59] J.R. Lakowicz, Principles of Fluorescence Spectroscopy, Plenum, New York, 1999.

[60] C.D. Mackay, R.N. Tubbs, R. Bell, D. Burt, P. Jerram, I. Moody, Sub-electron read noise at MHz pixel rates, in: SPIE Proc., Vol. 4306, 2001, pp. 289–298.

[61] K. Kemnitz, L. Pfeifer, R. Paul, M. Coppey-Moisan, Novel detectors for fluorescence lifetime imaging on the picosecond time scale, J. Fluor. 7 (1997) 93–98.

[62] C.G. Hübner, V. Krylov, A. Renn, P. Nyffeler, U.P. Wild, Single-molecule fluorescence – each photon counts, in: R. Rigler, M. Orrit, T. Basche (Eds.), Book, Springer-Verlag, Stockholm, 2001.

[63] R.M. Dickson, A.B. Cubitt, R.Y. Tsien, W.E. Moerner, On/off blinking and switching behaviour of single molecules of green fluorescent protein, Nature 388 (1997) 355–358.

[64] H.P. Lu, X.S. Xun, L. Xie, Single-molecule enzymatic dynamics, Science 282 (1998) 1877–1882.

[65] G.S. Harms, L. Cognet, P.H.M. Lommerse, G.A. Blab, T. Schmidt, Autofluorescent proteins in single-molecule research: Applications to live cell imaging microscopy, Biophys. J. 80 (2001) 2396–2408.

[66] D.A. Vanden Bout, W.-T. Yip, D. Hu, D.-K. Fu, M.T. Swager, P.F. Barbara, Discrete intensity jumps and intramolcular electronic energy transfer in the spectroscopy of single conjugated polymer molecules, Science 277 (1997) 1074–1077.

[67] M. Wu, P.M. Goodwin, W.P. Ambrose, R.A. Keller, Photochemistry and fluorescence emission dynamics of single molecules in solution – B-phycoerythrin, J. Phys. Chem. 100 (1996) 17406–17409.

[68] M.A. Bopp, Y. Jia, L. Li, R.J. Cogdell, R.M. Hochstrasser, Fluorescence and photobleaching dynamics of single light-harvesting complexes, Proc. Nat. Acad. Sci. USA 94 (1997) 10630–10635.

[69] J. Hofkens, W. Schroeyers, D. Loos, M. Cotlet, F. Köhn, T. Vosch, M. Maus, A. Herrmann, K. Müllen, T. Gensch, F.C. De Schryver, Triplet states as non-radiative traps in mulichromophoric entities: single molecule spectroscopy of an artificial and natural antenna system, Spectr. Acta A 57 (2001) 2093–2107.

[70] S.A. Empedocles, D.J. Norris, M.G. Bawendi, Photoluminescence spectroscopy of single CdSe nanocrystallite quantum dots, Phys. Rev. Lett. 77 (1996) 3873–3876.

[71] T. Ha, T. Enderle, D.S. Chemla, P.R. Selvin, S. Weiss, Quantum jumps of single molecules at room temperature, Chem. Phys. Lett. 271 (1997) 1–5.

[72] J.A. Veerman, M.F. Garcia-Parajo, L. Kuipes, N.F. van Hulst, Time-varying triplet state lifetimes of single molecules, Phys. Rev. Lett. 83 (1999) 2155–2158.

[73] A.L. Efros, M. Rosen, Random telegraph signal in the photoluminescence intensity of a single quantum dot, Phys. Rev. Lett. 78 (1997) 1110–1113.

[74] U. Banin, M. Bruchez, A.P. Alivisatos, T. Ha, S. Weiss, D.S. Chemla, Evidence for a thermal contribution to emission intermittency in single CdSe/CdS core/shell nanocrystals, J. Chem. Phys. 110 (1999) 1195–1201.

[75] T. Ha, T. Enderle, D.S. Chemla, S. Weiss, Dual-molecule spectroscopy: Molecular rulers for the study of biological macromolecules, IEEE J. Sel. Topics Quantum Electron. 2 (1996) 1115–1128.

[76] S.X. Xie, R.C. Dunn, Probing single molecule dynamics, Science 265 (1994) 361–364.

[77] T. Ha, T. Enderle, D.S. Chemla, P.R. Selvin, S. Weiss, Single molecule dynamics studied by polarization modulation, Phys. Rev. Lett. 77 (1996) 3979–3982.

[78] W.P. Ambrose, P.M. Goodwin, J.C. Martin, R.A. Keller, Alterations of single molecule fluorescence lifetimes in near-field optical microscopy, Science 265 (1994) 364–367.

[79] H. Gersen, M.F. Garcia-Parajo, L. Novotny, J.A. Veerman, L. Kuipers, N.F. van Hulst, Influencing the angular emission of a single molecule, Phys. Rev. Lett. 85 (2000) 5312–5315.

[80] C. Eggeling, S. Berger, L. Brand, J.R. Fries, J. Schaffer, A. Volkmer, C.A.M. Seidel, Data registration and selective single-molecule analysis using multi-parameter fluorescence detection, J. Biotechnol. 86 (2001) 163–180.

[81] T. Ha, T.A. Laurence, D.S. Chemla, S. Weiss, Polarization spectroscopy of single fluorescent molecules, J. Phys. Chem. B 103 (1999) 6839–6850.

[82] J.N. Forkey, M.E. Quinlan, Y.E. Goldman, Protein structural dynamics by single-molecule fluorescence polarization, Prog. Biophys. Mol. Biol. 74 (2000) 1–35.

[83] F. Güttler, M. Croci, A. Renn, U.P. Wild, Single molecule polarization spectroscopy: pentacene in p-terphenyl, Chem. Phys. 211 (1996) 421–430.

[84] T. Ha, J. Glass, T. Enderle, D.S. Chemla, S. Weiss, Hindered rotational diffusion and rotational jumps of single molecules, Phys. Rev. Lett. 80 (1998) 2093–2096.

[85] R.M. Dickson, D.J. Norris, W.E. Moerner, Simultaneous imaging of individual molecules aligned both parallel and perpendicular to the optic axis, Phys. Rev. Lett. 81 (1998) 5322–5325.

[86] A.P. Bartko, R.M. Dickson, Imaging three-dimensional single molecule orientations, J. Phys. Chem. B 103 (1999) 11237–11241.

[87] B. Sick, B. Hecht, L. Novotny, Orientational imaging of single molecules by annular illumination, Phys. Rev. Lett. 85 (2000) 4482–4485.

[88] J. Azoulay, A. Débarre, R. Jaffiol, P. Tchénio, Original tools for single-molecule spectroscopy, Single Molecules 2 (2001) 241–249.

[89] P.R. Selvin, The renaissance of fluorescence resonance energy transfer, Nature Struct. Biol. 7 (1999) 730–734.

[90] T. Ha, Single-molecule fluorescence resonance energy transfer, Methods 25 (2001) 78–86.

[91] L. Stryer, R.P. Haugland, Energy transfer: A spectroscopic ruler, Proc. Nat. Acad. Sci. USA 58 (1967) 719–726.

[92] A. Grinvald, E. Haas, I.Z. Steinberg, Evaluation of the distribution of distances between energy donors and acceptors by fluorescence decay, Proc. Nat. Acad. Sci. USA 69 (1972) 2273–2277.

[93] E.J. Sanchez, L. Novotny, G.R.X.S.X. Holtom, Room-temperature fluorescence imaging and spectroscopy of single molecules by two-photon excitation, J. Phys. Chem. A 101 (1997) 7019–7023.

[94] M.A. Albota, C. Xu, W.W. Webb, Two-photon fluorescence excitation cross sections of biomolecular probes from 690 to 960 nm, Appl. Opt. 37 (1998) 7352–7356.

[95] P.S. Dittrich, P. Schwille, Photobleaching and stabilization of fluorophores used for single-molecule analysis with one- and two-photon excitation, Appl. Phys. B 73 (2001) 829–837.

[96] S. Nie, S.R. Emory, Probing single molecules and single nanoparticles with surface-enhanced raman scattering, Science 275 (1997) 1102–1106.

[97] K. Kneipp, H. Kneipp, I. Itzkan, R.R. Dasari, M.S. Feld, Surface-enhanced non-linear Raman scattering at the single-molecule level, Chem. Phys. 247 (1999) 155–162.

[98] H.P. Lu, X.S. Xie, Single-molecule kinetics of interfacial electron transfer, J. Phys. Chem. B 101 (1997) 2753–2757.

[99] R.A. Marcus, N. Sutin, Electron transfers in chemistry and biology, Biochem. Biophys. Acta 811 (1985) 265–322.

[100] H. Geerts, M. De Brabander, R. Nuydens, S. Geuens, M. Moeremans, J. De Mey, P. Hollenbeck, Nanovid tracking: a new automatic method for the study of mobility in living cells based on colloidal gold and video microscopy, Biophys. J. 52 (1987) 775–782.

[101] J. Gelles, B.J. Schnapp, M.P. Sheetz, Tracking kinesin-driven movements with nanometer scale precision, Nature 331 (1988) 450–453.

[102] N. Bobroff, Position measurement with a noise-limited instrument, Rev. Sci. Instrum. 57 (1986) 1152–1157.

[103] Y. Hiraoka, J.W. Sedat, D.A. Agard, Determination of three-dimensional imaging properties of a light microscope system, Biophys. J. 57 (1990) 325–333.

[104] P.H. Kao, A.S. Verkman, Tracking of single fluorescent particles in three dimensions: use of cylindrical optics to encode particle position, Biophys. J. 67 (1994) 1291–1300.

[105] M. Born, E. Wolf, Principles of Optics, Cambridge University Press, 1999.

[106] E. Betzig, Proposed method for molecular optical imaging, Opt. Lett. 20 (1995) 237–239.

[107] T.A. Klar, S. Jakobs, M. Dyba, A. Egner, S.W. Hell, Fluorescence microscopy with diffraction resolution barrier broken by stimulated emission, Proc. Nat. Acad. Sci. USA 97 (2000) 8206–8210.

[108] X. Michalet, T.D. Lacoste, S. Weiss, Ultrahigh-resolution colocalization of spectrally resolvable point-like fluorescent probes, Methods 25 (2001) 87–102.

[109] J. Kohler, J.A.J.M. Disselhorst, M.C.J.M. Donckers, E.J.J. Groenen, J. Schmidt, W.E. Moerner, Magnetic resonance of a single molecular spin, Nature 363 (1993) 242–244.

[110] J. Wrachtrup, C. von Borczyskowski, J. Bernard, M. Orrit, R. Brown, Optical detection of magnetic resonance in a single molecule, Nature 363 (1993) 244–245.

[111] C. Brunel, P. Tamarat, B. Lounis, J. Woehl, M. Orrit, Tark effect on single molecules of dibenzanthanthrene in a naphthalene crystal and in a *n*-hexadecane Shpol'skii matrix, J. Phys. Chem. A 103 (1999) 2429–2434.

[112] Y. Wai-Tak, H. Dehong, Y. Ji, D.A. Vanden Bout, P.F. Barbara, Lassifying the photophysical dynamics of single- and multiple-chromophoric molecules by single molecule spectroscopy, J. Phys. Chem. A 102 (1998) 7564–7575.

[113] C. Tietz, F. Jelezko, U. Gerken, S. Schuler, A. Schubert, H. Rogl, J. Wrachtrup, Single molecule spectroscopy on the light-harvesting complex II of higher plants, Biophys. J. 81 (2001) 556–562.

[114] S. Brasselet, W.E. Moerner, Fluorescence behavior of single-molecule pH-sensors, Single Molecules 1 (2000) 17–23.

[115] Y. Jia, D. Talaga, W. Lau, H. Lu, W. DeGrado, R. Hochstrasser, Folding dynamics of single GCN4 peptides by fluorescence resonant energy transfer confocal microscopy, Chem. Phys. 247 (1999) 69–83.

[116] X. Zhuang, L.E. Bartley, H.P. Babcock, R. Russell, T. Ha, D. Herschlag, S. Chu, A single-molecule study of RNA catalysis and folding, Science 288 (2000) 2048–2051.

[117] M. Nishiyama, E. Muto, Y. Inoue, T. Yanagida, H. Higuchi, Substeps within the 8-nm step of the ATPase cycle of single kinesin molecules, Nature Cell Biol. 3 (2001) 425–428.

[118] H. Sosa, E.J.G. Peterman, W.E. Moerner, S.B. Goldstein, ADP-induced rocking of the kinesin motor domain revealed by single-molecule fluorescence polarization microscopy, Nature Struct. Biol. 8 (2001) 540–544.

[119] K. Adachi, R. Yasuda, H. Noji, H. Itoh, Y. Harada, M. Yoshida, K. Kinosita, Stepping rotation of F1-ATPase visualized through angle-resolved single-fluorophore imaging, Proc. Nat. Acad. Sci. USA 97 (2000).

[120] H. Taguchi, T. Ueno, H. Tadakuma, M. Yoshida, T. Funatsu, Single-molecule observation of protein–protein interactions in the chaperonin system, Nature Biotech. 19 (2001) 861–865.

[121] R. Yasuda, H. Noji, M. Yoshida, K. Kinosita, H. Itoh, Resolution of distinct rotational substeps by submillisecond kinetic analysis of F1-ATPase, Nature 410 (2001) 898–904.

[122] A.A. Deniz, T.A. Laurence, G.S. Beligere, M. Dahan, A.B. Martin, D.S. Chemla, P.E. Dawson, P.G. Schultz, S. Weiss, Single-molecule protein folding: Diffusion fluorescence resonance energy transfer studies of the denaturation of chymotrypsin inhibitor 2, Proc. Nat. Acad. Sci. USA 97 (2000) 5179–5184.

[123] Y. Sako, S. Minoguchi, T. Yanagida, Single-molecule imaging of EGFR signalling on the surface of living cells, Nature Cell Biol. 2 (2000) 168–172.

643

[124] R. Iino, I. Koyama, A. Kusumi, Single molecule imaging of green fluorescent proteins in living cells: E-cadherin forms oligomers on the free cell surface, Biophys. J. 80 (2001) 2667–2677.

[125] G.S. Harms, L. Cognet, P.H.M. Lommerse, G.A. Blab, H. Kahr, R. Gamsjäger, H.P. Spaink, N.M. Soldatov, C. Romanin, T. Schmidt, Single-molecule imaging of L-type Ca^{2+} channels in live cells, Biophys. J. 81 (2001) 2639–2646.

[126] M. Ueda, Y. Sako, T. Tanaka, P. Devreotes, T. Yanagida, Single-molecule analysis of signaling in dictyostelium cells, Science 294 (2001) 864–867.

[127] G. Seisenberger, M.U. Ried, T. Endreß, H. Büning, M. Hallek, C. Bräuchle, Real-time single-molecule imaging of the infection pathway of an adeno-associated virus, Science 294 (2001) 1929–1932.

[128] D. Axelrod, Total internal reflection fluorescence microscopy in cell biology, Traffic 2 (2001) 764–774.